



Lifetime prediction of turbine blades using global precipitation products from satellites

Merete Badger¹, Haichen Zuo¹, Ásta Hannesdóttir¹, Abdalmenem Owda¹, Charlotte Hasager¹

5 ¹Department of Wind and Energy Systems, Technical University of Denmark, Roskilde, 4000, Denmark

Correspondence: Merete Badger (mebc@dtu.dk)

Abstract. The growing size of wind turbines leads to extremely high tip speeds when the blades are rotating. The blades are prone to leading edge erosion when raindrops hit the blades at such high speeds and blade damage will eventually affect the power production until repair or replacement of the blade is performed. Since these actions come with a high cost, it is relevant to estimate the blade lifetime for a given wind farm site prior to wind farm construction. Modelling tools for blade lifetime prediction require input time series of rainfall intensities and wind speeds in addition to a turbine-specific tip speed curve. In this paper, we investigate the suitability of satellite-based precipitation data from the Global Precipitation Measurement (GPM) Mission in the context of blade lifetime prediction. We first evaluate satellite-based rainfall intensities from the Integrated Multi-Satellite Retrievals for GPM (IMERG) final product against in situ observations at 18 weather stations located in Germany, Denmark, and Portugal. We then use the satellite and in situ rainfall intensities as input to a model for blade lifetime prediction together with the wind speeds measured at the stations. We find that blade lifetimes estimated with rainfall intensities from satellites and in situ observations are in good agreement despite the very different nature of the observation methods and the fact that IMERG products have a 30 minute temporal resolution whereas in situ stations deliver 10 minute accumulated rainfall intensities. Our results indicate that the wind speed has a large impact on the estimated blade lifetimes. Inland stations show significantly longer blade lifetimes than coastal stations, which are more exposed to high mean wind speeds. One station located in mountainous terrain shows large differences between rainfall intensities and blade lifetimes based on satellite and in situ observations. IMERG rainfall products are known to have a limited accuracy in mountainous terrain. Our analyses also confirm that IMERG overestimates light rainfall and underestimates heavy rainfall. Given that networks of in situ stations have large gaps over the oceans, there is a potential for utilizing rainfall products from satellites to estimate and map blade lifetimes. This is useful as more wind power is installed offshore including floating installations very far from the coast.

1 Introduction

Leading edge erosion is a progressive roughening of wind turbine blades caused by the impact of precipitation with the blade movement through the air. The problem is evidently more pronounced offshore than for wind farms on land. Blade lifetimes of only 5-7 years have been reported for offshore wind farms in the North Sea even though the nominal lifetime of a turbine blade is typically 20-25 years (Ibrahim and Medraj, 2020; Herring et al., 2019). Leading edge erosion of wind turbine blades is a relatively new challenge. It has emerged with the growing rotor diameter of modern wind turbines, which leads to higher tip speeds.

A newly installed turbine blade has an incubation time where no damage is observed. Thereafter, initial damage occurs in the form of pinholes. Widespread damage will follow and it can be observed as an erosion of material in the top coating, filler or substrate. Repair of the blade is typically scheduled long before structural damage occurs. A rough blade has poorer aerodynamic efficiency and therefore, leading edge roughness can cause a significant loss of the annual wind power production (Bak et al., 2020). It can



lead to unforeseen operation and maintenance (O&M) cost (Mishnaevsky and Thomsen, 2020) and, eventually, to replacement of wind turbine blades. O&M is costly offshore and contributes to the operational expenditures (OPEX) of a given wind farm. A strategy to mitigate this financial risk is to operate the turbines in a so-called erosion safe mode during events of heavy precipitation and strong winds (Bech et al., 2018; Skrzypiński et al., 2020).

In connection with the planning of offshore wind energy projects, it is essential to predict the lifetime of the turbine blades in order to estimate the OPEX during the project lifetime. To calculate the lifetime of a wind turbine blade, information about the rainfall intensity and wind speed at the wind turbine location is needed at the highest possible temporal and spatial resolution. The temporal coverage of the rain and wind data sets should ideally be on the order of ten years to account for intra-annual variabilities (Hasager et al., 2021). Additional information about the wind turbine tip speed curve is also necessary since the movement of the turbine blade relative to that of the raindrops and the wind direction is determining the blade damage.

Networks of rain gauges and rain radars are established on land; typically by national meteorological agencies (Kidd et al., 2017). The rain observations are used for many different applications e.g. hydrology, agriculture, health, civil protection, and climate change monitoring. In contrast, rain observations over the oceans are very sparse (Klepp et al., 2020) and rain information is typically obtained through Numerical Weather Prediction (NWP) modeling or satellite observations (Shaw et al., in review). Previous blade lifetime analyses are based on rain gauge observations (Bech et al., accepted; Hasager et al., 2020; 2021; Law and Koutsos, 2020; Skrzypiński et al., 2020; Verma et al., 2021a), disdrometer observations (Tilg et al., 2022; Verma et al., 2021b), weather radar observations (Letson et al., 2020), re-analysis data (Prieto and Karlsson, 2021), and mesoscale weather model outputs (Eisenberg et al., 2018; Visbeck et al., in review).

The Global Precipitation Measurement (GPM) mission is a network of satellites delivering global rain observations since 2014 (Hou et al., 2014). It has a Core Observatory consisting of dual-frequency precipitation radars operating in Ku-band (13.6 GHz) and Ka-band (35.5 GHz), as well as the GPM Microwave Imager; a radiometer operating at different frequencies from 10 to 183 GHz. Many other spaceborne microwave sensors contribute to GPM and additional observations from infrared sensors on geostationary satellites are included. The GPM mission is an expansion of the Tropical Rainfall Measuring Mission (TRMM), which was in operation during 1997-2015 (Huffman et al., 2007). Whereas TRMM sensed the heavy rainfall associated within the tropics, GPM is also sensing the light rain, hail, and snowflakes common to higher latitudes. Here, we hypothesize that rainfall intensities from GPM can also be useful for the prediction of erosion damage on wind turbine blades; especially offshore where no other rain observations exist.

Integrated Multi-Satellite Retrievals for GPM (IMERG) lead to global level-3 rain products with a uniform grid spacing of 0.1° latitude and longitude from latitude 60°N to latitude 60°S. The temporal sampling of these products is 30 minutes. The initial sampling of the different satellite sensors contributing to IMERG can be considerably higher or lower and therefore, the IMERG validation performance varies for different scales, periods, and locations on Earth (Chen and Li, 2016). IMERG products come in three versions: early, late, and final. The final product is considered the most suitable for scientific applications as it includes assimilation of rain gauge observations from the Global Precipitation Climatology Centre. Therefore, it compares best with independent in situ observations (Tapiador et al., 2020). Dezfuli et al. (2017) find that the IMERG final product outperforms the previous TRMM Multisatellite Precipitation Analysis. Thanks to the higher temporal and spatial resolution of IMERG, the product captures mesoscale convective systems much better.



The objective of this paper is to determine whether rainfall intensities obtained from the IMERG final product are suitable for estimating the lifetime of wind turbine blades. The idea of using satellite data for blade lifetime prediction was put forward by Mishnaevsky et al. (2021) and here we test its applicability in practice. We first evaluate the performance of IMERG rainfall intensities with respect to high quality in situ observations from weather stations. Next, we use the IMERG and in situ observations of the rainfall intensity as input to a damage model code for prediction of blade lifetimes and compare the two types of lifetime estimates.

2 Previous evaluations of the IMERG final product

A number of independent studies evaluate the performance of IMERG final products for different regions, temporal scales, and applications. Overall, IMERG tends to overestimate light rain intensities and underestimate heavy rain intensities. This can lead to seasonal biases for regions where the rain characteristics vary throughout the year (Bogerd et al., 2021; Maranan et al., 2020; Tapiador et al., 2020). Rios Gaona et al. (2016) perform an early evaluation of the IMERG final product against ground based rain radar observations in the Netherlands and finds that IMERG underestimates countrywide rainfall depths by 2%.

90

Based on comparisons with rain gauge data in Brazil, Freitas et al. (2020) find that the IMERG product is a good source of sub-daily rainfall depth data for hydrological and hydroclimatic applications but they find large overestimations and underestimations of the IMERG product for rainfall duration and intensity properties, respectively. Cui et al. (2020) focus on mesoscale convective systems in the US and report that IMERG overestimates the total annual precipitation but underestimates the hourly mean precipitation. They note that evaporation of light rain under clouds causes frequent false alarms and positive biases (i.e. IMERG shows precipitation pixels but no rain is measured at the ground stations). A very high number of false alarms (83% of all IMERG rain pixels) is also reported by Maranan et al. (2020) for forested areas in Ghana, whereas high rain intensities are negatively biased.

95

A decomposition according to the source of the IMERG data can give insights in the performance per sensor type. Based on analyses over the eastern United States, Tan et al. (2016) find that the detection of rain events is most reliable for passive microwave sensors or morphed products whereas infrared sensors alone lead to a poorer performance when it comes to identification of rain events. Infrared sensors miss a very large fraction of the actual rain events measured on the ground. Bogerd et al. (2021) find that false alarm rates are amplified when infrared sensors are included in an analysis over the Netherlands.

105

For detected rain events, the performance on rain rate estimates also varies from sensor to sensor (Bogerd et al., 2021). For all data sources, the intensity of shallow rainfall is the most challenging to estimate and work is ongoing to improve the algorithms for detection and classification of such events (Arulraj and Barros, 2017). Mountainous terrain represents another challenge for accurate rainfall detection from microwave instruments due to rain-shadowing (Prakash et al., 2018).

110 3 Data

Figure 1 shows the areas of interest for this analysis, which covers 18 meteorological stations in Germany, Denmark and Portugal.

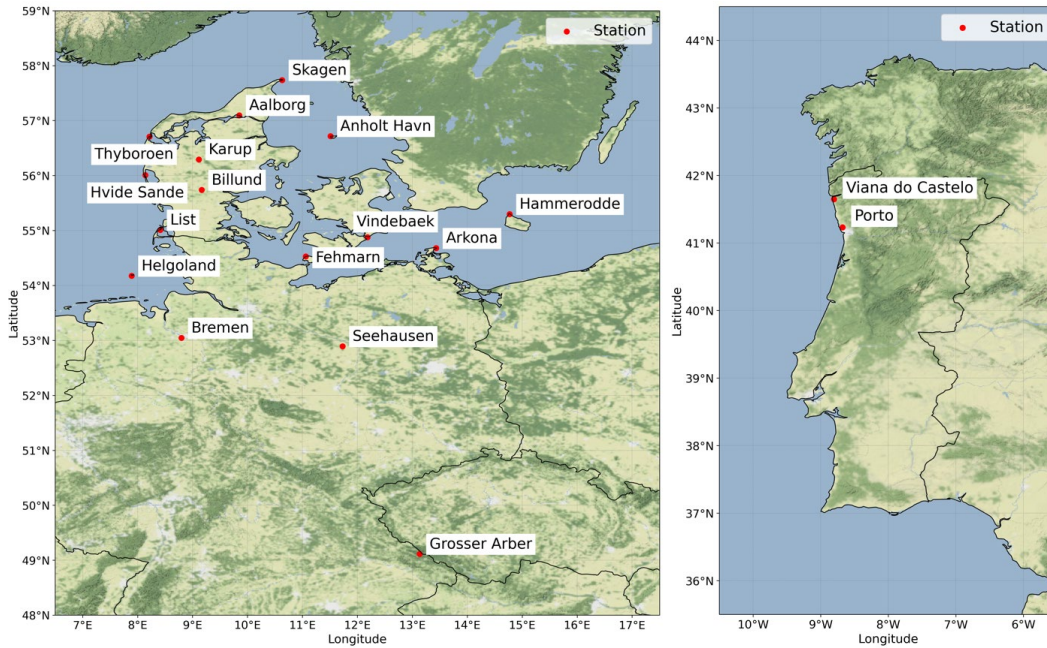


Figure 1. Locations of the 18 meteorological stations investigated. Left: Stations in Germany and Denmark; right: stations in
115 Portugal (© Stamen Design).

3.1 Satellite observations

Satellite observations of rainfall intensities are obtained from the product called GPM IMERG Final Precipitation L3 Half Hourly 0.1 degree x 0.1 degree V06 (GPM_3IMERGHH) (Huffman et al., 2019). We choose the IMERG final product for estimation of
120 the turbine blade erosion because it is calibrated with rain gauge measurements and has better data quality (Huffman et al., 2020).

We investigate the period from 2014 to 2019. GPM data are included in the IMERG Final product from February 2014, and in situ data are available for all stations during the six-year period. Based on nonparametric tests, IMERG data of January 2014 show a good consistency with the data from the rest of the period. So we carry out the study for the six complete years. We extract time
125 series of the parameters *precipitationCal* (i.e. precipitation estimate in mm/hr based on multi-satellite with gauge calibration) together with *precipitationQualityIndex* (i.e. a quality index for the precipitationCal field) and *probabilityLiquidPrecipitation* (i.e. the probability of liquid precipitation phase in percent) for the grid cell over each meteorological station.

3.2 In situ observations

We obtain observations of rainfall intensity and wind speed for 12 coastal and 6 inland stations located in Germany (7), Denmark
130 (9), and Portugal (2). Locations of the meteorological stations are shown in Figure 1. The German data series are obtained from the German Weather Service (DWD), the Danish data series are obtained from the Danish Meteorological Institute (DMI), and the Portuguese data series are obtained from the Portuguese Institute for Sea and Atmosphere (IPMA). The German and Danish stations have been used in previous works by Bech et al. (accepted) and Hasager et al. (2021) where detailed descriptions are given.



135 Rainfall intensities are measured by rain gauges at each meteorological station and quality control is performed; see Hasager et al. (2020; 2021) for details. The rainfall intensities are delivered as 10 minute cumulative values. In order to match the temporal resolution of the rainfall intensities from IMERG, we calculate the cumulative values over 30 minute intervals.

140 Wind speeds and directions at the meteorological stations are observed at the height 10 m except at Grosser Arber and Seehausen where winds are measured at 15 m height and at Arkona where the measurement height is 24 m. We extrapolate the wind speeds to the hub-height of the IEA 15 MW turbine (Gaertner et al., 2020) using the wind profile power law with the alpha exponent of 0.143 following Hsu et al. (1994). The same method is applied in Bech et al. (accepted) and Hasager et al. (2021). To collocate the in situ observations with the IMERG product in time, we average the 10 minute wind speeds and directions to 30 minute intervals.

4 Methods

145 4.1 Data pre-processing

For the IMERG product, we remove *precipitationCal* data whenever *precipitationQualityIndex* is smaller than 0.4 to ensure a sufficient data quality (Huffman et al., 2020). We only consider the impact of rain on wind turbine blades so instances where solid precipitation (hail, sleet and snow) occur are filtered out. We keep values if the parameter *probabilityLiquidPrecipitation* is larger than 0.7. Solid precipitation is also removed from the in situ data set.

150

After quality control, we convert the IMERG data to half-hourly accumulated rainfall. Since IMERG data is based on instantaneous rainfall intensity, for temporal collocation, we split the 10 minute in situ rainfall to 5 minute intervals and then accumulate them from 15 minutes before to 15 minutes after the IMERG measurement time, as shown in Figure 2. After collocation, the data availability for blade erosion estimation is shown in Figure 3.

155

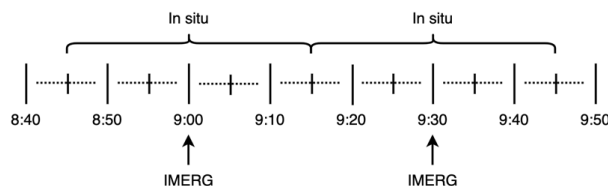
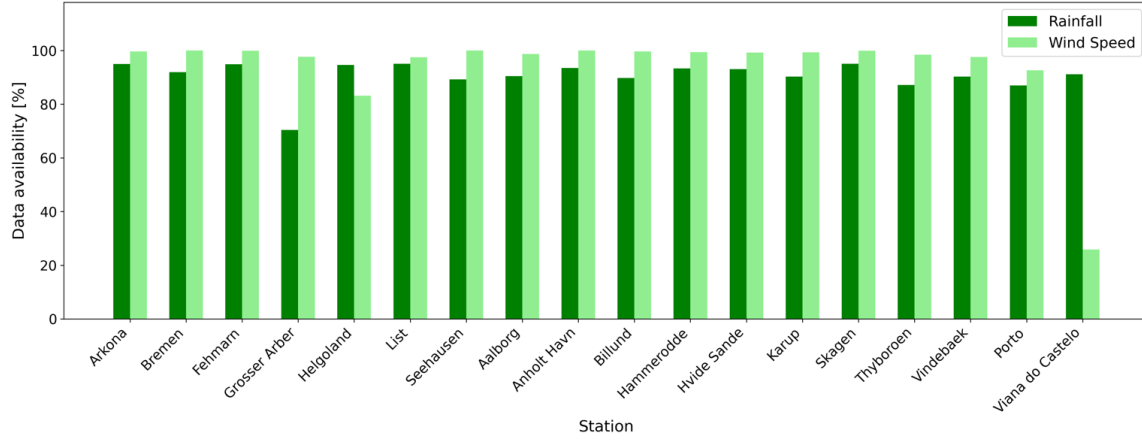


Figure 2. Time collocation between IMERG and in situ rainfall intensities.



160 Figure 3. Availability of IMERG and in situ data after quality control and collocation.

4.2 IMERG data evaluation

We evaluate the data quality of the IMERG product by comparing with in situ measurements. Referring to the existing established statistics (Bogerd et al., 2021), the relative bias (RB), mean absolute error (MAE), and normalized MAE ($NMAE$) are calculated for each station based on Eq. (1), (2) and (3):

165

$$RB = \frac{\sum_{i=1}^n (R_{IMERG,i} - R_{In situ,i})}{\sum_{i=1}^n R_{In situ,i}} \times 100\% \quad (1)$$

$$MAE = \frac{\sum_{i=1}^n |R_{IMERG,i} - R_{In situ,i}|}{n} \quad (2)$$

170

$$NMAE = \frac{\sum_{i=1}^n |R_{IMERG,i} - R_{In situ,i}|}{\sum_{i=1}^n R_{In situ,i}} \quad (3)$$

where $R_{IMERG,i}$ and $R_{In situ,i}$ are the 30 minute rainfall accumulation for the IMERG product and in situ measurements, respectively; n is the sample size over the whole study period or corresponding to a certain condition, such as rainfall intensity.

175 Contingency metrics, including the probability of detection (POD) and the probability of false alarm ($POFA$), are also quantified based on Eq. (4) and (5) (Bogerd et al., 2021):

$$POD = \frac{hits}{hits + misses} \quad (4)$$

180

$$POFA = \frac{false\ alarms}{hits + false\ alarms} \quad (5)$$

where “hits”, “misses” and “false alarms” are defined in Table 1. The threshold to distinguish whether there is rainfall during a 30 minute interval is 0.1 mm.



185

Table 1. Definition of thresholds for “hit”, “miss” and “false alarm” (mm/30 minutes).

Item	R_{IMERG}	$R_{in situ}$
Hit	≥ 0.1	≥ 0.1
Miss	< 0.1	≥ 0.1
False alarm	≥ 0.1	< 0.1

Apart from the overall comparisons, the temporal variability of rainfall intensities is also assessed. Correlation coefficients (R) based on daily rainfall between the two measurement systems are calculated for each country according to Eq.(6):

190

$$R = \frac{\sum_{i=1}^n (R_{IMERG-d,i} - \overline{R_{IMERG-d}})(R_{In situ-d,i} - \overline{R_{In situ-d}})}{\sqrt{\sum_{i=1}^n (R_{IMERG-d,i} - \overline{R_{IMERG-d}})^2 \sum_{i=1}^n (R_{In situ-d,i} - \overline{R_{In situ-d}})^2}} \quad (6)$$

195

where $R_{IMERG-d,i}$ and $R_{In situ-d,i}$ are the daily rainfall for the IMERG product and ground-based measurements, respectively; $\overline{R_{IMERG-d}}$ and $\overline{R_{In situ-d}}$ are the mean daily rainfall of a country for the IMERG product and ground-based measurements, respectively; i is the day, and n is the total number of days during the study period. The monthly and annual variations of both rainfall intensity and wind speed over the whole study period are also quantified for each station.

200

To investigate the performance of IMERG under different rainfall intensities, we classify the rain rate into three categories: slight ($< 0.5 \text{ mm/h}$), moderate ($0.5 \sim 4 \text{ mm/h}$), heavy ($\geq 4 \text{ mm/h}$) (Met Office, 2022). For each category, the relative bias (RB) of each station is quantified according to Eq.(1).

205

4.3 Blade lifetime model

210

The impingement blade lifetime model (Bech et al., accepted) using the soft-sign fit for the drop sizes is used to estimate blade lifetimes at each of the stations. The model is based on the correlation between the drop size of impinging rain and the damage of the blade. The correlation is found from extensive tests of specimen in a rain erosion tester spun with several speeds and with four different drop sizes. Thus it is based on experimental data. The impingement model is sensitive to the tip speed, the rainfall intensity, and the drop size. We assume that an IEA 15 MW turbine is installed at each of the in situ stations and we predict the lifetime of its blade. The rainfall intensity is observed by IMERG and in situ and both data sets are used as input together with the in situ wind speed. Wind speeds are extrapolated to the hub-height of the IEA 15 MW wind turbine (150 m) and converted to tip speed. The median drop size is estimated from the function of Best (1950) from the rainfall intensities from IMERG and the in situ observations. The model output is a lifetime in years for the blades on the fictive 15 MW turbine.

5 Results

5.1 IMERG data evaluation

In the following, we present the results of comparing the IMERG final product against in situ observations at the 18 stations in Germany, Denmark, and Portugal.



215 **5.1.1 Overall comparison of IMERG and in situ rainfall intensities**

Table 2 shows the overall statistics of comparisons between the IMERG and in-situ observations per station calculated for the ‘hits’ (i.e. times where both IMERG and the in situ stations show rainfall). The mean rainfall intensities from IMERG are higher than the observed values for all stations except for Grosser Arber in Germany. Subsequently, we find positive *RB* values for 17 stations. Grosser Arber is the only station in our data set, which is located far inland and in mountainous terrain and this could be the reasons why it deviates from the other stations. *MAE* ranges from 0.7 mm to 1.3 mm. Considering that the mean rainfall per station is on the same order of magnitude, this *MAE* is high as also reflected in the *NMAE* values ranging from 0.8 to 1.5. Our findings are similar to those reported in Bogerd et al. (2021) for the Netherlands.

The metric *POD* is an expression of the number of hits relative to all hits and misses. It would have the value 1 if all rain events observed at the in situ stations were detected correctly by IMERG. For the stations investigated here, *POD* lies within the range of 0.4-0.6. *POFA*, on the other hand, expresses the number of false alarms relative to all hits and false alarms. It would have the value 0 if all rain events detected by IMERG were also observed by the in situ stations. *POFA* lies within the range 0.4-0.7 in our analysis. *POD* and *POFA* are well correlated ($R^2 = 0.88$) so stations with a high *POD* also show a high *POFA*.

230 Table 2. Overall statistics of comparisons between the IMERG and in situ observations of accumulated rainfall during 30 minute periods in 2014-19. Only hits are considered for the calculation of mean values, relative biases (*RB*), Mean Absolute Errors (*MAE*) and Normalized Mean Absolute Errors (*NMAE*). *POD* is the Probability of Detection and *POFA* is the Probability of False Alarms.

Site	IMERG mean (mm)	In situ mean (mm)	RB (%)	MAE (mm)	NMAE -	POD -	POFA -
Arkona	1.2	0.6	89.0	0.9	1.5	0.6	0.7
Bremen	1.0	0.7	45.4	0.8	1.1	0.5	0.6
Fehmarn	0.9	0.7	40.6	0.7	1.1	0.5	0.6
Grosser Arber	0.8	1.1	24.6	0.9	0.8	0.5	0.6
Helgoland	1.0	0.7	50.0	0.8	1.2	0.6	0.6
List	1.2	0.7	83.3	0.9	1.4	0.5	0.6
Seehausen	1.0	0.8	21.6	0.7	1.0	0.5	0.6
Aalborg	1.0	0.6	60.0	0.7	1.2	0.4	0.5
Anholt Havn	1.1	0.6	73.1	0.8	1.3	0.6	0.6
Billund	1.3	0.8	67.1	1.0	1.2	0.4	0.4
Hammerodde	0.9	0.6	40.6	0.7	1.1	0.5	0.6
Hvide Sande	1.3	0.7	96.4	1.0	1.5	0.5	0.6
Karup	1.3	0.7	84.2	1.0	1.3	0.4	0.4
Skagen	1.4	0.7	94.4	1.1	1.5	0.6	0.7
Thyboroen	1.2	0.7	64.1	0.9	1.3	0.5	0.5
Vindebaek	0.9	0.6	41.7	0.7	1.1	0.5	0.6
Porto/Pedras Rubas	1.4	1.2	16.2	1.3	1.1	0.5	0.5
Viana do Castelo/Chafé	1.4	1.0	30.6	1.2	1.1	0.5	0.5

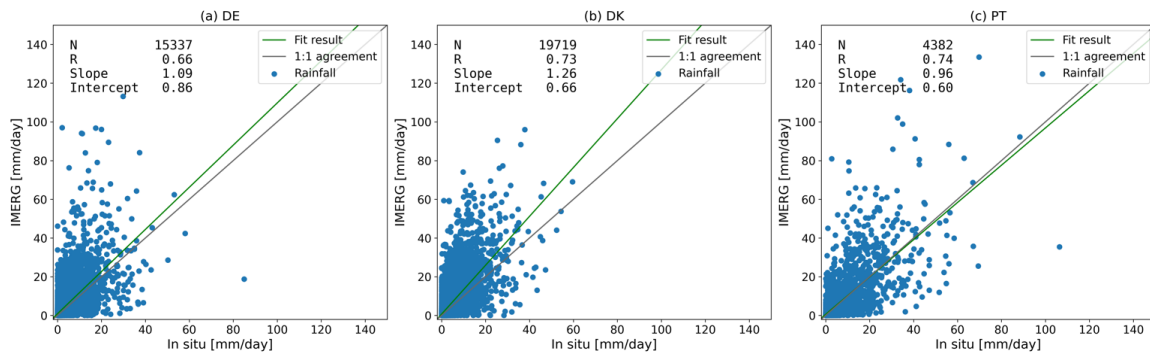


5.1.2 Temporal variability of rainfall intensities

To obtain a deeper understanding of the statistics presented above, we examine the temporal variability of the rainfall intensities detected from IMERG and the in situ stations. We consider the daily, monthly, and annual variability of the rainfall intensities.

240 Daily variability

Figure 4 shows scatter plots of the daily accumulated rainfall values from IMERG vs. in situ observations for the period 2014-19. We separate the German, Danish, and Portuguese stations since the in situ data originate from national weather services in each respective country. It is possible that procedures for quality control and filtering of the data vary between these agencies. Further, the climatic conditions may vary from country to country. All three plots show a clear linear relationship between IMERG and in situ rainfall intensities with a positive intercept, which is a direct consequence of the positive RB values presented in Table 2. We also notice a number of outliers in each plot where the IMERG data set shows extremely high rainfall intensities, which do not occur in the in situ data set, and vice versa.



250 **Figure 4.** Scatter plots showing the rainfall intensities from IMERG vs. the in situ observations during the period 2014-19 for a) German stations, b) Danish stations, and c) Portuguese stations. Each data point represents a daily accumulated value.

Figure 5 shows time series of the daily rainfall intensities per station for the example year 2019. The overall impression is that peaks in the time series from IMERG coincide in time with peaks measured at the in situ stations. This indicates, once again, that rainy days are detected from both time series. In case the rainfall on a given day falls in different 30 minute periods for IMERG and the in situ stations, it will contribute to the *POD* and *POFA* statistics given above. The magnitude of peaks can be very different between the two data sets. The time series from Arkona, Helgoland, List, Anholt Havn, Skagen, Porto/Pedras Rubas, and Viana do Castelo/Chafé show occasional spikes where the rainfall intensity from IMERG exceeds 80 mm. These high rates are not reflected in the in situ observations. At Grosser Arber and Porto/Pedras Rubas we see examples of rainfall events exceeding 80 mm in the in situ data where the IMERG data show more moderate intensities.

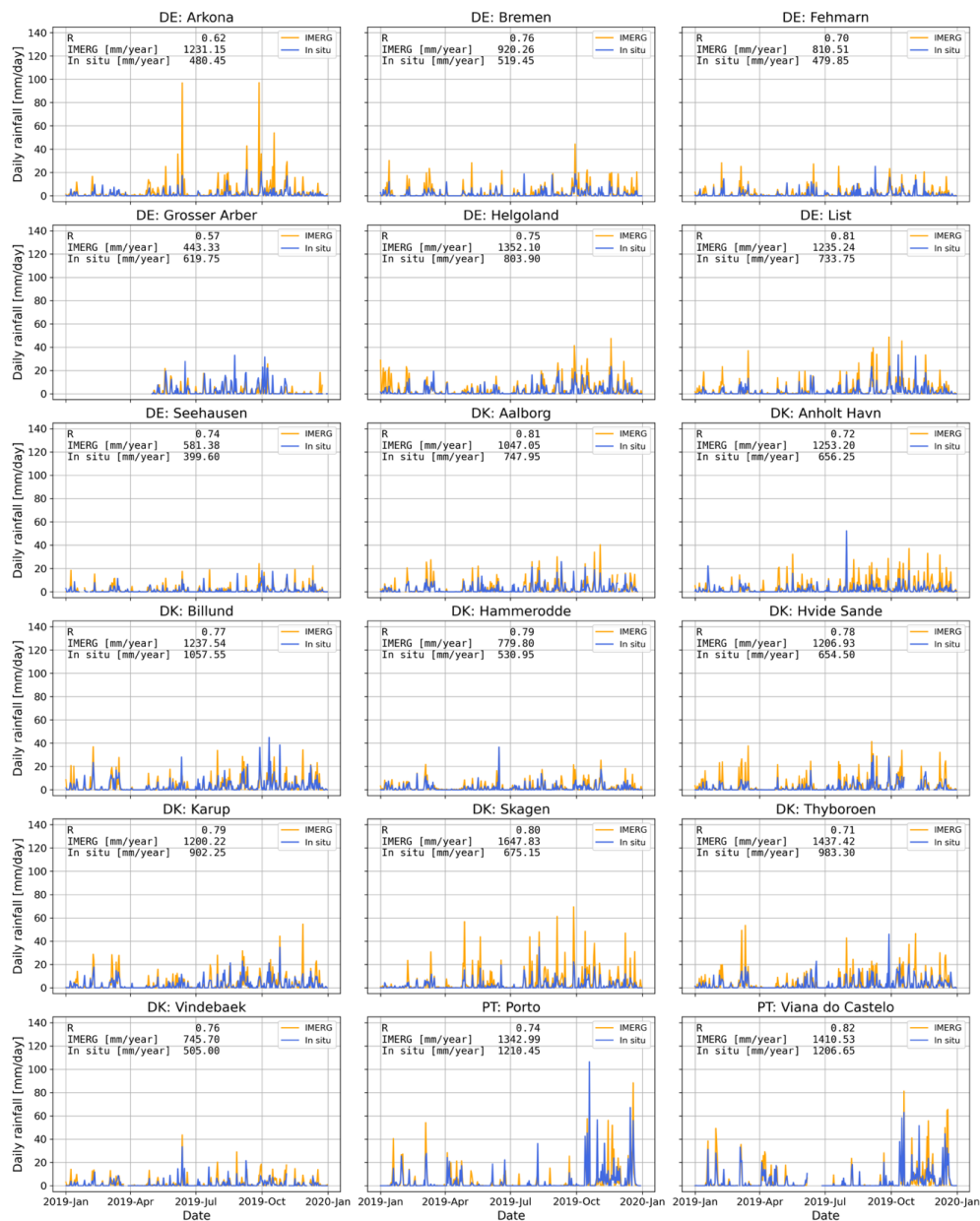


Figure 5. Daily rainfall intensities from IMERG and in situ observations during the example year 2019 for the 18 stations investigated.

265

Monthly variability

Figure 6 shows accumulated monthly rainfall intensities and monthly mean wind speeds per station averaged over 2014-19. Overall, the rain gauges in Germany and Denmark show the highest rainfall intensities during the summer months with peaks in July, August, or September and often with a secondary maximum during the winter months. At the two Portuguese stations, in contrast, the summer is very dry and the rainfall intensities peak in November.

270



From Figure 6 it is also evident that there can be large differences between the monthly rainfall from IMERG and the in situ stations. IMERG overestimates the monthly rainfall with respect to the in situ observations at all stations except for Grosser Arber and the two Portuguese stations. At these stations, the in situ observations show higher monthly rainfall intensities than IMERG for
275 ~~some~~ months during June to October. The differences between IMERG and in situ rainfall vary throughout the year and are most likely related to the dominant type of rain at a given time of the year (Bogerd et al., 2021). We find the largest discrepancies between IMERG and in situ rainfall for the stations Arkona, Helgoland, List, Anholt Havn, Hvide Sande, and Skagen. Several of these stations also showed large peaks in the time series in Figure 5.

280 Most of the German and Danish stations show the highest mean wind speeds in the winter months; especially in December and January. The monthly wind speed variation is most pronounced for stations near the coast (Arkona, Fehmarn, Helgoland, List, Anholt Havn, Hammerodde, Hvide Sande, Skagen, and Thyborøn) whereas the monthly mean wind speeds observed at the inland stations are lower and more uniform throughout the year. The inland station Grosser Arber is an exception as it shows a similar
285 monthly wind speed distribution to the coastal stations. The reason for this deviation could be that Grosser Arber is located in mountainous terrain so the wind speed observations are influenced by topography. The two stations in Portugal show low mean wind speeds ($2-4 \text{ m s}^{-1}$) throughout the year so the wind climate is significantly different from that of the German and Danish stations.

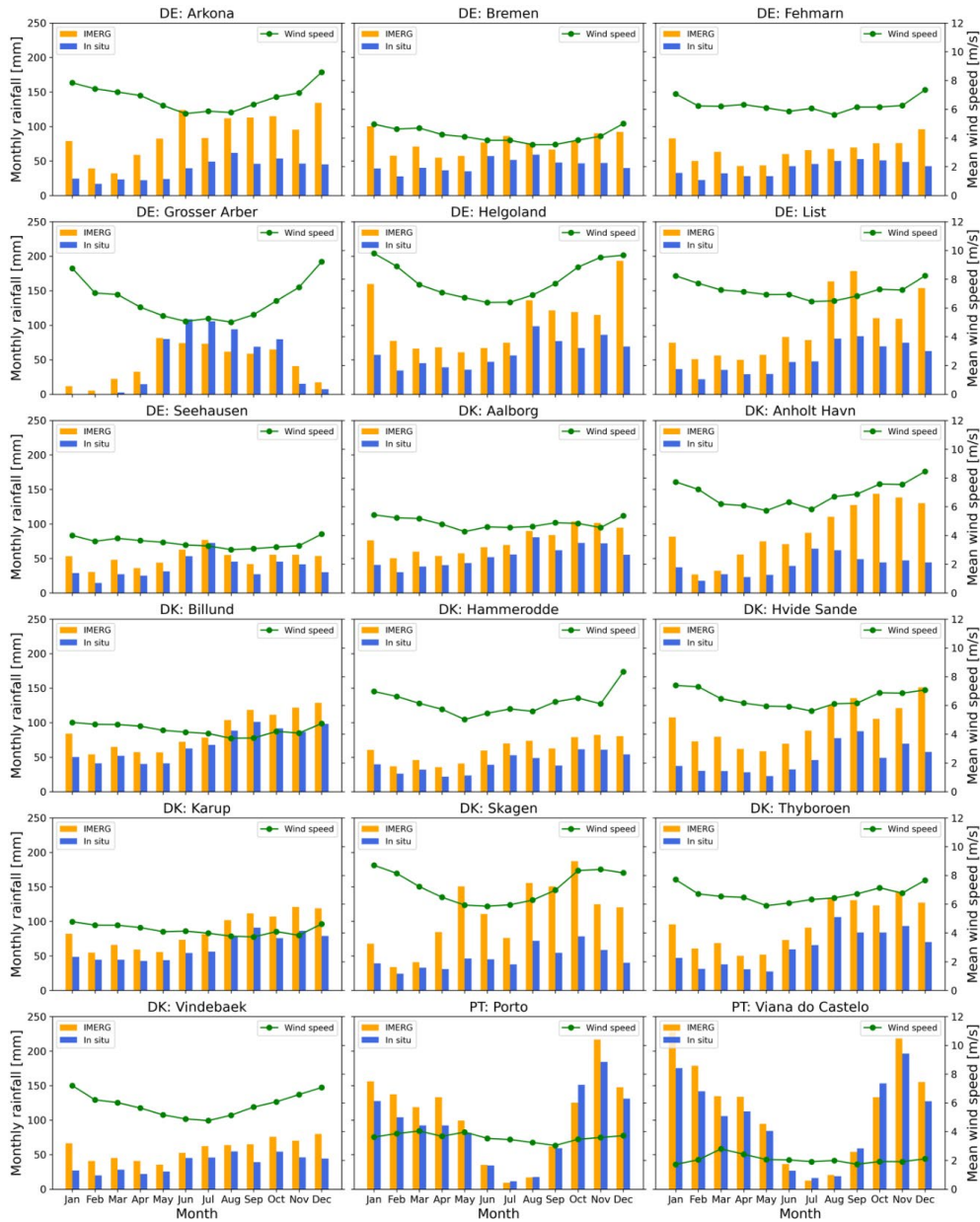


Figure 6. Monthly rainfall from IMERG and in situ observations (bars) and monthly mean wind speeds from in situ observations (green curves) averaged over 2014-19 for the 18 stations investigated.

Inter-annual variability

Figure 7 shows the accumulated annual rainfall and the mean wind speed per year for the 18 stations. The annual rainfall per station is also listed in Table 3. The annual rainfall intensities reflect the findings for daily and monthly timescales: At 16 stations, IMERG rainfall intensities exceed the intensities observed on the ground during all the six years investigated. At Grosser Arber, we find that the highest rainfall intensities are observed at the in situ stations for four of the years (2014, 2016, 2018, 2019) whereas IMERG



rainfall intensities are higher during 2015 and 2017. Viana do Castelo in Portugal shows a higher rainfall intensity from the in situ measurements during 2015 but for the other years, IMERG shows the highest intensities.

300 **Table 3.** Accumulated annual rainfall (mm) and average rainfall during 2014-19 from IMERG and in situ observations for the 18 stations investigated.

Station	Data set	2014	2015	2016	2017	2018	2019	Average
Arkona	IMERG	1182	1095	1022	1180	698	1231	1068
	In situ	500	519	392	548	271	480	452
Bremen	IMERG	904	1055	798	1095	672	920	907
	In situ	561	612	424	650	397	519	527
Fehmarn	IMERG	820	880	742	917	584	811	792
	In situ	502	522	415	582	350	480	475
Grosser Arber	IMERG	701	475	622	633	384	443	543
	In situ	816	401	662	549	409	620	576
Helgoland	IMERG	1161	1402	1082	1512	1037	1352	1258
	In situ	698	716	627	910	514	804	711
List	IMERG	1200	1597	943	1309	706	1235	1165
	In situ	681	688	481	721	394	734	617
Seehausen	IMERG	637	698	522	787	445	581	612
	In situ	526	487	345	597	294	400	441
Aalborg	IMERG	927	1036	800	923	707	1047	907
	In situ	570	744	540	766	484	748	642
Anholt Havn	IMERG	1076	1235	823	1309	774	1253	1079
	In situ	550	504	415	514	244	656	481
Billund	IMERG	1202	1244	954	976	699	1238	1052
	In situ	915	952	700	786	513	1058	821
Hammerodde	IMERG	797	763	627	869	525	780	727
	In situ	579	546	398	568	361	531	497
Hvide Sande	IMERG	1314	1426	999	1205	913	1207	1177
	In situ	666	669	460	527	432	655	568
Karup	IMERG	1144	1232	923	979	723	1200	1033
	In situ	777	865	582	819	525	902	745
Skagen	IMERG	1476	1398	1161	1248	890	1648	1303
	In situ	700	593	392	562	436	675	560
Thyboroen	IMERG	876	1338	990	1293	951	1437	1148
	In situ	526	851	544	829	686	983	736
Vindebaek	IMERG	765	835	645	770	428	746	698
	In situ	451	588	434	474	261	505	452
Porto/Pedras Rubas	IMERG	914	1046	1731	1036	1477	1343	1258
	In situ	898	920	1458	798	1238	1210	1087
Viana do Castelo/Chafé	IMERG	1872	1014	1583	989	1530	1411	1400
	In situ	1729	1050	1214	784	1327	1207	1218



Figure 7 also shows that fluctuations of the mean wind speed from year to year are limited during 2014-19. Mean wind speeds exceeding 6 m s^{-1} are found for stations located near the coast (Arkona, Fehmarn, Helgoland, List, Anholt Havn, Hammerodde, Hvide Sande, Skagen, and Thyborøn) whereas inland stations show lower mean wind speeds on the order of $4\text{-}6 \text{ m s}^{-1}$. Grosser Arber is again an exception as the mean wind speed here is $6\text{-}8 \text{ m s}^{-1}$. This is most likely due to the higher elevation of the station.



Figure 7. Annual rainfall from IMERG and in situ observations (bars) and annual mean wind speeds from in situ observations (green curves) during the period 2014-19 for the 18 stations investigated.



5.1.3 Bias of the rainfall intensity according to precipitation type

Relative biases (*RB*) on rainfall intensities for different precipitation types (i.e. slight, moderate, and heavy) are given in Table 4. The table shows that IMERG overestimates rainfall at slight and moderate intensities whereas rainfall at high intensities is underestimated for all 18 stations. This finding is well aligned with the literature (Bogerd et al.; 2021; Maranan et al. 2020; Tapiador et al., 2020) and also with the monthly distributions of rainfall presented in Figure 6.

Table 4. Relative biases (*RB*) of the rainfall intensity (mm) for different categories of precipitation: slight ($< 0.5 \text{ mm/h}$), moderate ($0.5 \sim 4 \text{ mm/h}$), heavy ($\geq 4 \text{ mm/h}$). Red colour indicates overestimation and blue colour underestimation of rainfall intensities by IMERG with respect to the in situ stations.

Site	Slight	Moderate	Heavy
Arkona	376.2	96.7	-5.0
Bremen	404.4	56.0	-50.6
Fehmarn	301.4	52.4	-41.0
Grosser Arber	243.7	-2.1	-60.1
Helgoland	362.6	55.0	-35.0
List	325.4	92.5	1.2
Seehausen	362.6	42.9	-49.1
Aalborg	353.8	67.4	-36.5
Anholt Havn	402.4	73.4	-25.7
Billund	505.0	79.6	-26.1
Hammerodde	278.5	46.4	-51.8
Hvide Sande	567.7	105.4	-28.2
Karup	475.1	93.4	-20.7
Skagen	465.7	101.8	-0.1
Thyboroen	414.4	83.1	-35.1
Vindebaek	310.7	51.8	-52.2
Porto	574.6	64.8	-43.2
Viana do Castelo	500.2	66.1	-33.7

5.2 Blade lifetime estimates

In the following, we present the blade lifetimes estimated with input rainfall intensities from IMERG and the in situ stations, respectively. One of the 18 stations investigated, Viana do Castello in Portugal, is left out of this analysis because the data availability of wind speeds at the station is only 24% whereas the other stations have a data availability of 70-95% (Fig. 3).



Figure 8 shows the expected average blade lifetimes in years per station calculated with input rainfall from IMERG and the in situ stations. Overall, we see a good agreement between estimates based on IMERG and in situ rainfall intensities. Biases between the estimates based on IMERG and in situ rainfall are positive for eight stations and negative for seven stations. Seven of the stations show lifetimes deviating by less than one year for the IMERG and in situ inputs. The other stations show deviations up to 30% and the deviation for Grosser Arber is exceptionally high (approximately 100%) as the lifetime estimate from IMERG and in situ data are 11.2 years and 5.6 years, respectively. **This deviation might be due to challenges associated with microwave sensing and rain-shadowing in mountainous terrain** (cf. Sect. 2 and Prakash et al. (2018)).

The station Seehausen shows much longer lifetimes than the other stations (44.5 years from IMERG and 35.5 years from in situ observations). **This can be attributed to the relatively low rainfall intensities in combination with low mean wind speeds throughout the year at this location** (Figure 6). Two other inland stations, Bremen and Karup, also show blade lifetimes exceeding 10 years based on the in situ observations. Overall, the estimated blade lifetimes tend to be longer for inland stations compared to stations near the coast and Grosser Arber is again an exception from this pattern. Recent work by Bech et al. (accepted) supports these findings.

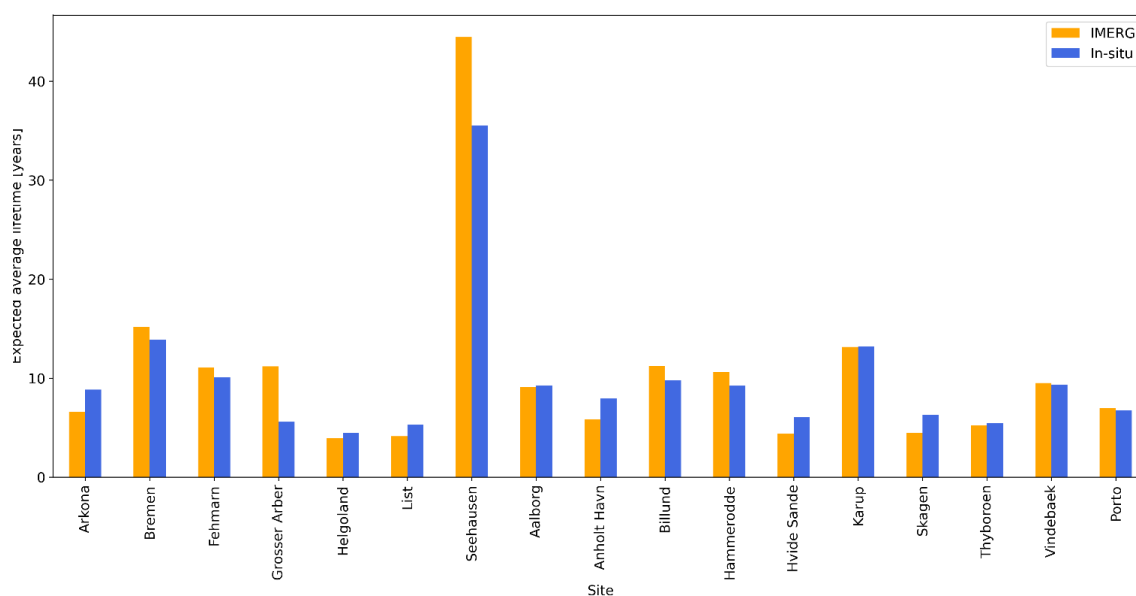


Figure 8. Blade lifetimes estimated using 30 minute accumulated rainfall intensities from IMERG and the in situ stations. Note that the Portuguese station Viana do Castelo is left out due to a limited wind data availability.

Rainfall intensities from IMERG are given as 30 minute accumulated values and we have created similar accumulated values from the in situ observations, whereas previous analyses over the same sites are based on the native 10 minute observations from the in situ observations (Bech et al., accepted). In order to test the sensitivity of blade lifetime estimates to the temporal resolution of the input rainfall intensities, we compare the estimated blade lifetimes based on 10 minute in situ observations with the lifetimes calculated with 30 minute accumulated rainfall. The outcome is shown in Figure 9, which indicates that the effect of accumulating the rainfall intensities to 30 minute values instead of using the native 10 minute values is small, i.e. ranging from -6% to 5% and



in absolute values from -0.4 years to 0.7 years. This is excluding Seehausen. At Seehausen the lifetime is very long and when we estimate lifetimes much longer than the length of our time series, the uncertainty increases.

355

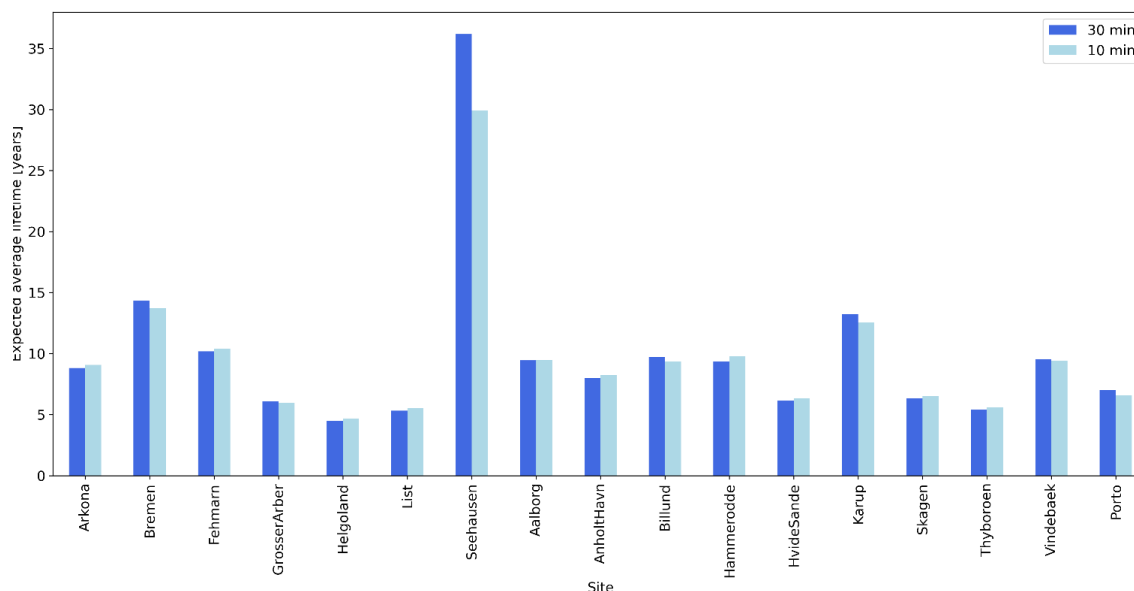


Figure 9. Blade lifetimes estimated using 30 minute accumulated rainfall intensities from the in situ stations and the native 10 minute rainfall intensities observed at the stations. Note that the Portuguese station Viana do Castelo is left out due to a limited wind data availability.

360 6 Discussion

This study is the first to use IMERG rain data as input to predict turbine blade lifetimes. Our blade lifetime estimates based on the IMERG final product data and local rain gauge data differ very little. This is a comforting fact as IMERG products are available onshore and offshore for more than eight years (2014-22). This could enable a regional to global mapping of the expected lifetime for specific turbines and blade coatings based on the concept applied here. In the context of blade lifetime assessment, the temporal coverage of available input data is important since the joint rain and wind variability in northern Europe is significant (Figure 7). Around 10 years of data is sufficient to predict blade lifetimes (Hasager et al., 2021). In case of shorter time series, there is considerable variation in the predicted lifetime. Our sensitively analysis using 10 minute vs. 30 minute accumulated rainfall intensities shows little influence on lifetime estimates at sub-hourly timescales. We see large differences for the station Seehausen only, which has a lifetime much longer than the length of our timeseries.

370

Our results suggest that blade lifetimes are shorter for locations near the coast as compared to stations located further inland. It is also evident that the wind speed plays a very important role when it comes to leading edge erosion as also shown by Bech et al. (accepted). The damage of turbine blades is caused by heavy rainfall and strong winds in combination and therefore, the coastal stations with high annual mean wind speeds are the most prone to damage of the turbine blades. This is in line with results from the Netherlands (Verma et al., 2021b).

375



Our comparisons of rainfall intensities from the IMERG final product versus rain gauge observations at ground stations confirm the findings in **previous works** (Bogerd et al., 2021). Light rainfall is overestimated by IMERG whereas **heavy rainfall is underestimated**. We see this pattern for all the 18 stations investigated (Table 4). We also find that the seasonal variability of the rainfall type and intensity drives the bias on IMERG rainfall rates with respect to in situ observations (Figure 6). Comparisons between IMERG and in situ observations of rainfall intensities are therefore only representative for local areas where the climatic conditions remain similar. Another reason why validation of the IMERG final product is representative for local areas only is the nature of the data set where the number and the type of satellite sensors as well as the number of in situ stations assimilated in the product is variable (cf. Sect. 1).

385

The stations considered here are primarily located in northern Europe where the rainfall conditions are similar in terms of the monthly distribution of rainfall (Figure 6) and the total amount of rainfall per year (Table 3). We therefore also find that the bias between IMERG and in situ rainfall is on the same order of magnitude (Table 2). The two stations in Portugal and the elevated station Grosse Arber are located in very different regimes in terms of rainfall. In spite of these differences, the bias between IMERG and in situ rainfall is not so different.

390

A few aspects should be noted about the reference precipitation data set used here as well as in previous works (Bech et al., accepted; Hasager et al., 2021). Networks of in situ stations operated by national weather services (here by DMI, DWD and IPMA) are primarily established to monitor extreme rain events and to model the hydrological balance of catchment areas. In connection with these activities, different corrections are implemented but such corrections are not necessarily included in the in situ data sets we have accessed. The in situ data set used here represents the best possible estimates of the rainfall intensities and wind speeds locally at the stations but they are not **perfect**. For example, strong winds may influence the amount of rainfall collected by a rain gauge. Such a bias will vary from station to station depending on the local wind climate. Likewise, the observations of wind speed may be influenced by sheltering obstacles such as buildings in the vicinity of the stations.

400

Precipitation measurements made with rain gauges at ground stations are very different in nature from remote sensing observations based on microwave or infrared sensors in space. Firstly, the observations are made at different levels in the atmosphere where the properties of a given rainfall event may also differ. Secondly, the sensing techniques are radically different. Rain gauges collect rain droplets by weight whereas remote sensing instruments in this context measure the properties of a volume of air. As described in Sect. 2, the capability of microwave sensors when it comes to detection of rainfall depends on the instrument frequency.

405

In our analyses, we have considered liquid precipitation only. Solid precipitation in the form of hail can cause severe damage on wind turbine blades as well (Letson et al., 2020; Macdonald et al., 2016). In the future, it might be possible to separate different types of precipitation with confidence and analyse their individual effects on leading edge erosion. Thanks to dual frequency Ku/Ka-band radar sensing in combination with passive microwave sensing, GPM makes it possible to estimate particle size distributions within rain clouds (Le and Chandrasekar, 2014; Tokay et al., 2017). Drop size distributions are essential for the development and prediction of storms. Tilg et al. (2022) have shown that the drop size distributions obtained from disdrometers (i.e. laser instruments) can also lead to improved estimates of the kinetic energy, which drives the leading edge erosion of turbine blades. The kinetic energy model used by Hasager et al. (2020, 2021), Skrzypiński et al. (2020), and Tilg et al. (2022) severely overestimates the effect of larger drops compared to smaller drops in contrast to the droplet-dependent impingement model used

415



in the present study (Bech et al., accepted). There is thus an obvious potential for resolving drop size distributions from GPM and using them for the prediction of blade lifetimes.

7 Conclusion

The combination of heavy rain and strong winds can cause leading edge erosion of wind turbine blades and ultimately, a need for blade repair or replacement. We have demonstrated for the first time that rainfall intensities obtained from the Global Precipitation Measurement (GPM) Mission constellation of satellites can be used as input for the prediction of blade lifetimes at locations in Germany, Denmark and Portugal. Our analysis is based on precipitation data from the Integrated Multi-Satellite Retrievals for GPM (IMERG) final product, which contains GPM observations since 2014. The satellite-based rainfall intensities were first compared against in situ observations of rainfall at the daily, monthly, and annual timescales. In line with previous analyses, we find that heavy rainfall is underestimated by IMERG whereas light rainfall is overestimated. The accuracy of annual rainfall intensities from IMERG is thus very dependent on the rainfall regime at a given point location and on the type(s) of satellite sensors and the number of ground stations included in the IMERG final product at that specific location. In spite of these challenges, blade lifetimes estimated from the satellite and in situ observations of rainfall are rather similar at most of the stations analyzed. We also find that the 30 minute temporal resolution offered by IMERG is sufficient to predict blade lifetimes. Our analyses indicate that there is a potential for using satellite-based rainfall observations for modeling of leading edge erosion and this represents a new application of the GPM. The findings are particularly relevant for planning of wind farms offshore where networks of in situ stations lack coverage. In the future, it might be possible to refine the analyses presented here by resolving the drop size distributions based on GPM satellite observations.

Data availability. IMERG final products are available for download at https://disc.gsfc.nasa.gov/datasets/GPM_3IMERGHH_06/summary.

Author contributions. MB coordinated the work and downloaded the IMERG final product. HZ compared rainfall and wind speed datasets from IMERG and in situ observations and made Figures 2-7. AH estimated blade lifetimes and made Figures 8- 9. AO prepared the IMERG time series and produced overview maps of the in situ stations (Figure 1). CH conceptualized the work, supervised the process, and acquired the financial support for the project leading to this publication. MB prepared the manuscript with contributions from all co-authors.

Competing interests. The authors declare that they have no conflict of interest.

Acknowledgements. We acknowledge the Goddard Earth Sciences Data and Information Services Center (GES DISC) for the GPM IMERG Final Precipitation product (Huffman et al., 2019) and the Danish Meteorological Institute (DMI), the Portuguese Institute for Sea and Atmosphere (IPMA) and the Open Data Server from Deutscher Wetterdienst (DWD) for meteorological data. The work presented here has received financial support by the Blade Defect Forecasting project funded by the Innovation Fund Denmark Grant 9067-00008B and by the Atlantic Regional Initiative – Applications: Offshore Wind Energy funded by the European Space Agency. The droplet dependent damage model for lifetime prediction is developed in the EROSION project funded by the Innovation Fund Denmark Grant 6154-00018B. Haichen Zuo is supported by the project LIKE (Lidar Knowledge Europe) H2020-MSCA-ITN-2019, Grant number 858358 funded by the European Union. Abdalmenem Owda has received funding



from the European Union's Horizon 2020 research and innovation programme under the Marie Skłodowska-Curie grant agreement
455 no. 861291 (Train2Wind).

References

- Arulraj, M., and Barros, A. P.: Shallow precipitation detection and classification using multifrequency radar observations and model simulations, *Journal of Atmospheric and Oceanic Technology*, 34(9), 1963–1983, <https://doi.org/10.1175/JTECH-D-17-0060.1>, 2017.
- 460 Bak, C., Forsting, A. M., and Sørensen, N. N.: The influence of leading edge roughness, rotor control and wind climate on the loss in energy production, *Journal of Physics: Conference Series*, 1618(5), 052050, <https://doi.org/10.1088/1742-6596/1618/5/052050>, 2020.
- Bech, J. I., Hasager, C.B., and Bak, C.: Extending the life of wind turbine blade leading edges by reducing the tip speed during extreme precipitation events, *Wind Energy Science*, 3, 729–748, <https://doi.org/10.5194/wes-3-729-2018>, 2018.
- 465 Bech, J.I., Johansen, N. F.-J., Madsen, M.B., Hannesdóttir, Á., and Hasager, C.B.: Experimental Study on the Effect of Drop Size in Rain Erosion Test and on Lifetime Prediction of Wind Turbine Blades, *Renewable Energy*, https://papers.ssrn.com/sol3/papers.cfm?abstract_id=4011160, accepted.
- Best, A.C.: The size of distribution of raindrops, *Quart. J. R. Met. Soc.*, 76, 16, 1950.
- Bogerd, L., Overeem, A., Leijnse, H., and Uijlenhoet, R.: A Comprehensive Five-Year Evaluation of IMERG Late Run
470 Precipitation Estimates over the Netherlands, *Journal of Hydrometeorology*, 22(7), 1855–1868, [10.1175/JHM-D-21-0002.1](https://doi.org/10.1175/JHM-D-21-0002.1), 2021.
- Chen, F., and Li, X.: Evaluation of IMERG and TRMM 3B43 monthly precipitation products over mainland China, *Remote Sensing*, 8(6), 472, <https://doi.org/10.3390/rs8060472>, 2016.
- Cui, W., Dong, X., Xi, B., Feng, Z. H. E., and Fan, J.: Can the GPM IMERG final product accurately represent MCSs?
475 precipitation characteristics over the central and eastern United States?, *Journal of Hydrometeorology*, 21(1), 39–57, <https://doi.org/10.1175/JHM-D-19-0123.1>, 2020.
- Dezfuli, A. K., Ichoku, C. M., Mohr, K. I., and Huffman, G. J.: Precipitation characteristics in West and East Africa from satellite and in situ observations, *Journal of Hydrometeorology*, 18(6), 1799–1805, <https://doi.org/10.1175/JHM-D-17-0068.1>, 2017.
- 480 Eisenberg, D., Laustsen, S., and Stege, J.: Wind turbine blade coating leading edge rain erosion model: Development and validation, *Wind Energy*, 21, 942–951, <https://doi.org/10.1002/we.2200>, 2018.
- Freitas, E. da S., Coelho, V. H. R., Xuan, Y., Melo, D. de C. D., Gadelha, A. N., Santos, E. A., ... Almeida, C. das N.: The performance of the IMERG satellite-based product in identifying sub-daily rainfall events and their properties, *Journal of Hydrology*, 589, 125128, <https://doi.org/10.1016/j.jhydrol.2020.125128>, 2020.
- 485 Gaertner, E.; Rinker, J.; Sethuraman, L.; Zahle, F.; Anderson, B.; Barter, G.; Abbas, N.; Meng, F.; Bortolotti, P.; Skrzypiński, W.R.; et al.: Definition of the IEA 15-Megawatt Offshore Reference Wind Turbine (NREL/TP-5000-75698); National Renewable Energy Laboratory: Golden, CO, USA. Available online: <https://www.nrel.gov/docs/fy20osti/75698.pdf>, 2020.
- Hasager, C.B., Vejen, F., Bech, J. I., Skrzypiński, W. R., Tilg, A.-M., and Nielsen, M.: Assessment of the rain and wind climate
490 with focus on wind turbine blade leading edge erosion rate and expected lifetime in Danish Seas, *Renewable Energy*, 149, 91–102, <https://doi.org/10.1016/j.renene.2019.12.043>, 2020.



- Hasager, C. B., Vejen, F., Skrzypinski, W. R., and Tilg, A.-M.: Rain Erosion Load and Its Effect on Leading edge Lifetime and Potential of Erosion-Safe Mode at Wind Turbines in the North Sea and Baltic Sea, *Energies*, 14(7), 1959, <https://doi.org/10.3390/en14071959>, 2021.
- 495 Herring, R., Dyer, K., Martin, F., and Ward, C.: The increasing importance of leading edge erosion and a review of existing protection solutions, *Renewable and Sustainable Energy Reviews*, 115, 109382, <https://doi.org/10.1016/j.rser.2019.109382>, 2019.
- Hou, A. Y., Kakar, R. K., Neeck, S., Azarbarzin, A. A., Kummerow, C. D., Kojima, M., ... Iguchi, T.: The global precipitation measurement mission, *Bulletin of the American Meteorological Society*, 95(5), 701–722, <https://doi.org/10.1175/BAMS-D-13-00164.1>, 2014.
- 500 Hsu, S. A., Meindl, E. A., and Gilhousen, D. B.: Determining the Power-Law Wind-Profile Exponent under Near-Neutral Stability Conditions at Sea, *Journal of Applied Meteorology and Climatology*, 33(6), 757-765, [https://doi.org/10.1175/1520-0450\(1994\)033<0757:DTPLWP>2.0.CO;2](https://doi.org/10.1175/1520-0450(1994)033<0757:DTPLWP>2.0.CO;2), 1994.
- Huffman, G., Bolvin, D., Nelkin, E. and Tan, J.: Integrated Multi-satellitE Retrievals for GPM (IMERG) Technical Documentation. [online] NASA. Available at: <https://gpm.nasa.gov/resources/documents/IMERG-V06-Technical-Documentation> [Accessed 11 March 2022], 2020.
- 505 Huffman, G. J., Bolvin, D. T., Nelkin, E. J., Wolff, D. B., Adler, R. F., Gu, G., Hong, Y., Bowman, K. P., Stocker, E. F.: The TRMM Multisatellite Precipitation Analysis (TMPA): Quasi-Global, Multiyear, Combined-Sensor Precipitation Estimates at Fine Scales, *J. Hydrometeorol.*, 8(1), 38-55, [10.1175/JHM560.1](https://doi.org/10.1175/JHM560.1), 2007.
- 510 Huffman, G. J., Stocker, E. F., Bolvin, D. T., Nelkin, E. J. and Tan, J.: GPM IMERG Final Precipitation L3 Half Hourly 0.1 degree x 0.1 degree V06, Greenbelt, MD, Goddard Earth Sciences Data and Information Services Center (GES DISC), Accessed: 08 February 2022, [10.5067/GPM/IMERG/3B-HH/06](https://doi.org/10.5067/GPM/IMERG/3B-HH/06), 2019.
- Ibrahim, M. E., and Medraj, M.: Water droplet erosion of wind turbine blades: Mechanics, testing, modeling and future perspectives, *Materials*, 13(1), 157, <https://doi.org/10.3390/ma13010157>, 2020.
- 515 Kidd, C., Becker, A., Huffman, G., Muller, C., Joe, P., Jackson, G., and Kirschbaum, D.: So, How Much of the Earth's Surface Is Covered by Rain Gauges?, *Bulletin of the American Meteorological Society*, 98, [10.1175/BAMS-D-14-00283.1](https://doi.org/10.1175/BAMS-D-14-00283.1), 2016.
- Klepp, C., Kucera, P.A., Burdanowitz, J., and Protat, A.: OceanRAIN – The Global Ocean Surface-Reference Dataset for Characterization, Validation and Evaluation of the Water Cycle. In: Levizzani, V., Kidd, C., Kirschbaum, D., Kummerow, C., Nakamura, K., and Turk, F. (eds): *Satellite Precipitation Measurement. Advances in Global Change Research*, vol 69, Springer, Cham, https://doi.org/10.1007/978-3-030-35798-6_10, 2020.
- 520 Law, H. and Koutsos, V.: Leading edge erosion of wind turbines: Effect of solid airborne particles and rain on operational wind farms, *Wind Energy*, 23, 10, 1955–1965, DOI: [10.1002/we.2540](https://doi.org/10.1002/we.2540), 2020.
- Le, M., and Chandrasekar, V.: An algorithm for drop-size distribution retrieval from GPM dual-frequency precipitation radar, *IEEE Transactions on Geoscience and Remote Sensing*, 52(11), 6813630, <https://doi.org/10.1109/TGRS.2014.2308475>, 2014.
- 525 Letson, F.; Barthelmie, R. J.; and Pryor, S. C.: Radar-derived precipitation climatology for wind turbine blade leading edge erosion, *Wind Energ. Sci.*, 5, 331–347, <https://doi.org/10.5194/wes-5-331-2020>, 2020.
- Macdonald, H., Infield, D., Nash, D. H. and Stack, M. M.: Mapping hail meteorological observations for prediction of erosion in wind turbines: UK hail meteorological observations, *Wind Energy* 19(4), 777–784, <https://doi.org/10.1002/we.1854>, 2016.
- 530



- Maranan, M., Fink, A. H., Knippertz, P., Amekudzi, L. K., Atiah, W. A., and Stengel, M.: A process-based validation of gpm imerg and its sources using a mesoscale rain gauge network in the west african forest zone, *Journal of Hydrometeorology*, 21(4), 729–749, <https://doi.org/10.1175/JHM-D-19-0257.1>, 2020.
- 535 Met Office: Fact sheet 3 — Water in the atmosphere. [ebook] Crown. Available at: <https://www.metoffice.gov.uk/research/library-and-archive/publications/factsheets> [Accessed 11 March 2022], 2012.
- Mishnaevsky Jr., L., Hasager, C.B., Bak, C., Tilg, A.-M., Bech, J. I., Rad, S.D., and Fæster, S.: Rain erosion of wind turbine blades: Understanding, prevention and protection, *Renewable Energy*, 169, 953–969, <https://doi.org/10.1016/j.renene.2021.01.044>, 2021.
- 540 Mishnaevsky, L. and Thomsen, K.: Costs of repair of wind turbine blades: Influence of technology 695 aspects, *Wind Energy*, 23, 2247–2255, <https://doi.org/10.1002/we.2552>, 2020.
- Prakash, S., Mitra, A. K., AghaKouchak, A., Liu, Z., Norouzi, H., and Pai, D. S.: A preliminary assessment of GPM-based multi-satellite precipitation estimates over a monsoon dominated region, *Journal of Hydrology*, 556, 865–876, <https://doi.org/10.1016/j.jhydrol.2016.01.029>, 2018.
- 545 Prieto, R., Karlsson, T.: A model to estimate the effect of variables causing erosion in wind turbine blades, *Wind Energy*, 24, 1031–1044, <https://doi.org/10.1002/we.2615>, 2021.
- Rios Gaona, M. F., Overeem, A., Leijnse, H., and Uijlenhoet, R.: First-year evaluation of GPM rainfall over the Netherlands: IMERG day 1 final run (V03D), *Journal of Hydrometeorology*, 17(11), 2799–2814, <https://doi.org/10.1175/JHM-D-16-0087.1>, 2016.
- 550 Shaw, W., Berg, L., Debnath, M., Deskos, G., Draxl, C., Ghate, V., Hasager, C., Kotamarthi, R., Mirocha, J., Muradyan, P., Pringle, W., Turner, D., and Wilczak, J.: Scientific Challenges to Characterizing the Wind Resource in the Marine Atmospheric Boundary Layer, *Wind Energ. Sci. Discuss.*, <https://doi.org/10.5194/wes-2021-156>, in review.
- Skrzypiński, W. R., Bech, J. I., Hasager, C. B., Tilg, A.-M., Bak, C., and Vejen, F.: Optimization of the erosion-safe operation of the IEA Wind 15 MW Reference Wind Turbine, *Journal of Physics: Conference Series*, 1618(5), 052034, <https://doi.org/10.1088/1742-6596/1618/5/052034>, 2020.
- 555 Tan, J., Petersen, W. A., and Tokay, A.: A novel approach to identify sources of errors in IMERG for GPM ground validation, *Journal of Hydrometeorology*, 17(9), 2477–2491, <https://doi.org/10.1175/JHM-D-16-0079.1>, 2016.
- Tapiador, F. J., Navarro, A., García-Ortega, E., Merino, A., Sánchez, J. L., Marcos, C., and Kummerow, C.: The contribution of rain gauges in the calibration of the IMERG product: Results from the first validation over Spain, *Journal of Hydrometeorology*, 21(2), 161–182, <https://doi.org/10.1175/JHM-D-19-0116.1>, 2020.
- 560 Tilg, A.-M., Skrzypiński, W. R., Hannesdóttir, Á., and Hasager, C. B.: Effect of drop-size parameterization and rain amount on blade-lifetime calculations considering leading edge erosion, *Wind Energy*, 25(5), 952–967, <https://doi.org/10.1002/we.2710>, 2022.
- Tokay, A., D'Adderio, L. P., Porcù, F., Wolff, D. B., and Petersen, W. A.: A field study of footprint-scale variability of raindrop size distribution, *Journal of Hydrometeorology*, 18(12), 3165–3179, <https://doi.org/10.1175/jhm-d-17-0003.1>, 2017.
- 565 Verma, A.S., Jiang, Z., Ren, Z., Caboni, M., Verhoef, H., van der Mijle-Meijer, H., ... Teuwen, J. J. E.: A probabilistic long-term framework for site-specific erosion analysis of wind turbine blades: A case study of 31 Dutch sites, *Wind Energy*, 24(11), 1315–1336, <https://doi.org/10.1002/we.2634>, 2021a.
- 570 Verma, A. S., Jiang, Z., Caboni, M., Verhoef, H., van der Mijle Meijer, H., Castro, S. G. P., and Teuwen, J. J. E.: A probabilistic rainfall model to estimate the leading-edge lifetime of wind turbine blade coating system, *Renewable Energy*, 178, 1435–1455, <https://doi.org/10.1016/j.renene.2021.06.122>, 2021b.

<https://doi.org/10.5194/wes-2022-59>
Preprint. Discussion started: 20 July 2022
© Author(s) 2022. CC BY 4.0 License.



Visbeck, J., Göçmen, T., Hasager, C. B., Shkalov, H., Handberg, M., and Nielsen, K. P.: Introducing a data-driven approach to predict site-specific leading edge erosion, *Wind Energ. Sci. Discuss.*, <https://doi.org/10.5194/wes-2022-55>, in review.